Published in final edited form as:
IEEE Trans Biomed Eng. 2011 June ; 58(6): 1629–1636. doi:10.1109/TBME.2011.2107515.

Detection of Vesicoureteral Reflux using Microwave Radiometry – System Characterization with Tissue Phantoms

Kavitha Arunachalam, **Paolo Maccarini**, **Valeria De Luca**, **Piero Tognolatti**, **Fernando Bardati**, **Brent Snow**, and **Paul Stauffer**

Abstract

Microwave (MW) radiometry is proposed for passive monitoring of kidney temperature to detect vesicoureteral reflux (VUR) of urine that is externally heated by a MW hyperthermia device and thereafter reflows from the bladder to kidneys during reflux. Here we characterize in tissue-mimicking phantoms the performance of a 1.375 GHz radiometry system connected to an electromagnetically (EM) shielded microstrip log spiral antenna optimized for VUR detection. Phantom EM properties are characterized using a coaxial dielectric probe and network analyzer (NA). Power reflection and receive patterns of the antenna are measured in layered tissue phantom. Receiver spectral measurements are used to assess EM shielding provided by a metal cup surrounding the antenna. Radiometer and fiberoptic temperature data are recorded for varying volumes (10–30 mL) and temperatures (40–46°C) of the urine phantom at 35 mm depth surrounded by 36.5°C muscle phantom. Directional receive pattern with about 5% power spectral density at 35 mm target depth and better than −10dB return loss from tissue load are measured for the antenna. Antenna measurements demonstrate no deterioration in power reception and effective EM shielding in the presence of the metal cup. Radiometry power measurements are in excellent agreement with the temperature of the kidney phantom. Laboratory testing of the radiometry system in temperature controlled phantoms supports the feasibility of passive kidney thermometry for VUR detection.

Index Terms

microwaves; radiometry; vesicoureteral reflux; tissue phantoms; noninvasive thermometry

I. INTRODUCTION

VUR is the abnormal flow of urine from the bladder to both or either kidneys. VUR is prevalent in 30% of the children diagnosed with urinary tract infection (UTI) [1]. Imaging studies currently recommended to detect reflux in children diagnosed with UTI involve bladder catheterization, sedation and ionizing radiation [2,3]. The unpleasant procedure and long term effect of ionizing radiation in infants and children [4,5] have motivated the development of alternative noninvasive imaging modalities for VUR detection [6]. The MW device proposed in [6] combines a 915 MHz hyperthermia applicator for external bladder warming to moderate temperatures (40–45°C) and MW radiometry to passively monitor the kidneys to detect the warm reflux. This alternative approach is noninvasive, non-ionizing and low cost, and does not require bladder catheterization or sedation. The total power radiometer connected to a tapered log spiral antenna inside a cylindrical metal cup reported in [6,7] is systematically characterized here in tissue equivalent phantoms.

Correspondence to: Kavitha Arunachalam.

NIH-PA Author Manuscript
NIH-PA Author Manuscript

The use of MW radiometry for passive temperature monitoring of deep tissues has been proposed in the literature for varied applications [8-11]. Among the most widely investigated applications are breast cancer detection [12-14], brain temperature monitoring in new born infants after hypoxia ischemia [15,16], tissue temperature monitoring for feedback power control of superficial hyperthermia [17-19] and interstitial MW applicators [20,21], and noninvasive thermometry for intracranial focused deep brain hyperthermia [22,23]. MW radiometry involves collecting thermal noise power emitted by the body in the EM spectrum (typically 1–4 GHz) using an antenna. The noise power received by the antenna over the band width Δf_i centered at frequency f_i is related to tissue temperature by [10],

$$P_i = kT_{B,i}\Delta f_i \tag{1}$$

where k is Boltzmann's constant and

$$T_{B,i} = (1-\rho_i)\int_V W(\vec{r}', f_i)T(\vec{r}')d+(1v-\rho_i)T_{EMI}+T_{sys} \tag{2}$$

is the radiometric brightness temperature. In (2), ρ_i is antenna power reflection coefficient, W is the antenna weighting function inside the sensing volume V, T_{EMI} is EM interference (EMI) noise collected by the antenna from the surroundings, and T_{sys} is receiver noise temperature. The radiometric weighting function $W=P_d\left(\int_v P_d dv\right)^{-1}$, is the power spectral density received by the antenna from the sensing volume normalized to the total collected power. In this work, we characterize the performance of a total power MW radiometer system with an EM shielded microstrip log spiral antenna in a phantom model that mimics the pediatric anatomy with kidney located below the layered fat and muscle tissues at 35 mm from the skin.

The organization of the paper is as follows. Section II describes the experimental setup, phantom formulations and spectral measurements of the radiometer and antenna. Radiometry experiments conducted for the urine target in tissue equivalent phantoms at varying depths, volumes and temperatures are also presented in section II. The results of EM characterization of tissue phantoms, antenna spectral power density, EM shielding provided by the metal cup and radiometer system response during kidney temperature monitoring are provided in section III. Finally, experimental results are discussed in section IV.

II. METHODS

A. Tissue Equivalent Phantoms

Several phantom formulations are available for biological models with tissue equivalent electromagnetic properties [24–26]. Clear and low viscous liquid phantoms that can be circulated through external temperature controlled water baths were formulated for the high water content muscle and kidney tissues over 0.9–2 GHz. Diethylene glycol monobutyl ether (DGBE) mixed with deionized water, 50% each by weight was used for the muscle tissue. A mixture of 33.5% Diacetin (glycerol diacetate), 65.5% deionized water and 1% salt (NaCl) by weight was formulated for the kidney tissue. A solid gelatin based fat phantom with 85% oil and 15% deionized water by weight was constructed for the fat tissue based on the recipe in [26]. The urine surrogate has 1.25% salt (NaCl) by weight in deionized water. The phantom materials were purchased from Fischer Scientific, Waltham, MA USA. EM properties of the tissue phantoms were characterized using a coaxial dielectric probe (E85070C, Agilent Technologies) connected to a network analyzer (E5071C, Agilent

Technologies). Phantom measurements were compared with Cole-Cole data for biological tissues [27] and the urine phantom was validated against human urine sample and literature data [20].

B. Experimental Setup

Due to similar dielectric properties of muscle and kidney tissues over the radiometer frequency band (1.1–1.65 GHz), the phantom model was constructed using liquid muscle inside 200×200×200 mm acrylic chamber with overlying 5 mm layer of solid fat. A 20 French, 3-way continuous irrigation Foley catheter (D in Fig 1) with two staggered drainage ports (Bard Medical Division, Covington, GA, USA) was modified to circulate variable volume of temperature controlled urine phantom inside the liquid muscle chamber. The urine phantom (C in Fig 1) was placed at various depths for temperature monitoring. An 18 French/2-way straight tip Foley catheter with 30 mL inflatable balloon (Bard Medical Division) was used for kidney reflux experiments to simulate varying volume warm urine reflow at depth using a syringe (J and K in Fig 1). The Foley catheter with urine phantom was rigidly fixed in position using a perforated hollow plastic post. Temperatures of the muscle and urine phantoms were separately controlled by circulating the phantoms through temperature controlled water baths using peristaltic pumps (Cole Parmer, Vernon Hills, IL USA). The muscle phantom was maintained at body core temperature of 36.5°C. Polystyrene slabs (Styrofoam®, Dow Chemicals, Midland, MA USA) were used to insulate the phantom container on all sides except the Mylar window. Fig 1 shows the experimental setup and accessories used for radiometric temperature monitoring of the tissue phantom.

A tapered microstrip log spiral antenna was used for passive temperature monitoring (E in Fig 1). Thin low loss dielectric matching disks of varying relative permittivity (F in Fig 1, Eccostock® HiK, Emmersons & Cuming Microwave Products, Randolph, MA USA) were used to decrease power reflection (ρ_i) at the interface between the antenna and tissue load. A cylindrical aluminum cup surrounding the antenna and matching layer shown in Fig 1 (G) was used to minimize EMI. The thermal noise power gathered by the EM shielded antenna was processed by a total power radiometer centered at 1.375 GHz with 550 MHz bandwidth and 0.03°C sensitivity. The radiometer consists of a single band very low noise receiver centered at 1.375 GHz connected to a commercial power meter (E4419B, Agilent Technologies, Santa Clara CA, USA) through a low power sensor (E4412A, Agilent Technologies) with dynamic range of −70 dBm to +20 dBm. Power received by the radiometer antenna is acquired in real time using GPIB interface. Phantom and antenna surface temperatures were continuously acquired during the experiments using fiberoptic temperature sensors (Luxtron 3100, LumaSense Technologies, Santa Clara, CA USA). Theoretical analysis of the design of log spiral antenna, radiometer frequency selection, and the use of matching layer and EM shield cup for VUR detection was reported in [7].

C. Antenna Measurements

1) EM Matching to Tissue load—Power reflection at the interface between the antenna and layered tissue phantom was measured for the microstrip log spiral antenna through the Mylar window. Reflection measurements were acquired using a network analyzer for 1 mm thick Eccostock® dielectric disks of varying permittivity (ε'=5–30) between the antenna and phantom to assess the amount of power coupled to the antenna from the tissue load. Antenna reflection measurements were used to select the appropriate dielectric matching layer between the antenna and tissue load for enhanced power reception.

2) EM Shielding of Metal cup—A cylindrical aluminum cup was placed around the antenna to minimize the effect of EMI on the low power radiometric signal received from the tissue phantom. The use of a metal cup surrounding the microstrip log spiral antenna for

EM shielding was originally proposed in [7]. The metal cup was in continuous contact with the antenna ground plane and the phantom surface as shown in Fig 1 (G). EM shielding provided by the metal cup was evaluated by measuring the radiometer spectral content in the presence and absence of metal cup with the antenna listening to the tissue load. Radiometer spectral measurements were obtained using a commercial spectrum analyzer (N9912A FieldFox, Agilent Technologies).

3) Antenna Receive Pattern—The 80 mm diameter microstrip log spiral antenna used in the radiometry experiments was fabricated on 1.524 mm thick dielectric substrate (RO4350B, Rogers Corporation Chandler, AZ USA) based on the design presented in [7]. The antenna receive pattern was characterized inside an acrylic tank (350×350×350 mm^3) filled with liquid muscle phantom and 100×100 mm Mylar window of 0.25 mm thickness for antenna placement. Antenna power spectral density was measured over 100×100×100 mm scan volume at 5 mm spatial interval in the muscle phantom using a scanning specific absorption rate (SAR) field probe (ALS-E010 Aprel Laboratories, Ottawa Canada). Antenna receive patterns were measured at 1.1, 1.3 and 1.6 GHz inside the radiometer frequency band. Measurements were also recorded for antenna inside the metal cup. Power delivered and reflected by the antenna was measured for all scan configurations using a network analyzer. Scan tank measurements were used to assess antenna power spectral density in muscle phantom and the effect of EM shield cup on power reception.

D. Radiometry Experiments

Information extracted from X-ray radiographs and computed tomography images of 4–8 year old were used to design the phantom experimental setup. The average thickness of fat layer was measured as 5 mm and the depth of urine reflux varied from 20–35 mm from skin surface with 10–30 mL reflux volume depending on the reflux grade. The distance between the front wall of the inflated Foley catheter with urine phantom and the antenna surface denoted as d_1 was varied. The distance between the isocenter of the inflated Foley catheter and antenna surface d_2 was fixed at 35 mm.

1) Steady State Temperature Monitoring—Simulated passive kidney temperature monitoring was performed by circulating 30 mL urine phantom (V_1 = 30 mL, d_1 = 18 mm, d_2 = 35mm) inside the modified 20 Fr Foley catheter with continuous irrigation ports. The depth, volume and temperature of the urine studied in this experiment are typical of high grade warm reflux (stages 3–5) in children ages 4–8 years with UTI. The muscle phantom surrounding the urine target was maintained at 36.5°C while the temperature of the urine phantom mimicking warm reflux at depth was changed by switching the heat exchange coil to a water bath 3–9°C above 36.5°C. The temperature of the circulating urine phantom was measured by inserting fiberoptic temperature sensors inside the irrigation ports of the Foley catheter. Invasive fiberoptic temperatures and passive radiometric signal gathered by the EM shielded microstrip antenna on the phantom Mylar window were continually recorded to assess the steady state system response.

2) Kidney Reflux Monitoring—The ability to detect sudden reflux of warm urine inside the kidneys was assessed by injecting a known volume of urine phantom (V_1) at initial temperature (T_0) inside the 18 Fr 2-way straight tip Foley catheter with 30 mL inflatable balloon rigidly held 35 mm (d_2) from the antenna surface. The average time required to inject and completely drain a known volume of urine phantom was 60 seconds. The temperature of the muscle phantom surrounding the Foley catheter was maintained at body core temperature of 36.5°C. Table 1 lists the experiments conducted for varying reflux volumes (V_1) and temperatures (T_0) of the urine phantom measured prior to injection. In Table 1, d_1 increases with decreasing reflux volume while d_2 remains at 35 mm.

III. RESULTS

A. Phantom Characterization

Fig 2 shows the relative permittivity and electrical conductivity of fat, muscle, kidney and urine phantoms in the radiometer frequency band measured at room temperature (23°C) using a coaxial probe connected to network analyzer. Cole-Cole dispersion data of biological tissues [27] are overlaid in Fig 2 at the radiometer center frequency (1.375 GHz). Phantom dielectric measurements are in good agreement with literature data for kidney and muscle phantoms with less than 6% error over the radiometer frequency band (1.1–1.65 GHz). The larger deviation observed for the solid fat phantom is due to the 15% water content used in the phantom formulation. Dielectric measurements of the urine phantom exhibit excellent agreement with human urine sample and literature data [20].

B. Antenna Measurements

1) EM Matching to Tissue Load—Fig 3 shows the antenna power reflection measurements ($|S_{11}|^2$) obtained with 1 mm thick Eccostock® dielectric disks of varying relative permittivity (ε'=5–30) placed between the antenna and tissue load through the Mylar window. Antenna reflection measurements indicate better than −10 dB over 1.1–1.9 GHz for most dielectric disks. A relatively smaller variation in $|S_{11}|^2$ and better than −10 dB response were observed across the entire radiometric band for the antenna coupled to the tissue phantom through the thin Mylar. Thus, the 0.25 mm thick Mylar window of relative permittivity ε'=3.2 was used as the matching layer for the phantom model although we expect the disks to accommodate the matching of the diverse anatomical scenarios in children.

2) Antenna EM Shielding—Fig 4 shows the radiometer power spectrum with the microstrip log spiral antenna listening to the layered phantom. Spectral measurements of Fig 4 were acquired in the presence and absence of the cylindrical aluminum cup surrounding the antenna. The metal cup was in continuous contact with the phantom surface and antenna ground plane. The radiometer power spectrum in the absence of the metal cup shows the potential in-band EMI noise. Comparison of the power spectrums demonstrates good EM shielding in the radiometer frequency band (1.1–1.65 GHz) in the presence of metal cup.

3) Antenna Receive Pattern—Fig 5a shows the power density distribution of the log spiral antenna at 1.3 GHz measured in the liquid muscle phantom. The electric field probe measurements were normalized with respect to the maximum value recorded in z=5 mm plane (z=0 corresponds to antenna surface). 3D isosurfaces of Fig 5a indicate directional receive pattern with less than 10% antenna power density at the target location (30–50 mm depth). Fig 5b shows the 5% isosurfaces measured at 1.1, 1.3 and 1.6 GHz in the radiometer frequency band. Comparison of the isosurfaces indicates a broader pattern at the lowest frequency (1.1 GHz) and a narrow pattern at the highest frequency (1.6 GHz), with no deterioration of the antenna receive pattern in the radiometric band.

Fig 6 shows the normalized antenna power density distributions in the orthogonal planes measured at 1.3 GHz in the presence and absence of metal cup surrounding the antenna. Power density distribution is normalized with respect to the maximum value in z=5 mm plane. Comparison of the power density depth profiles indicates no significant change in antenna receive pattern in the presence of the metal cup intended to minimize EMI. Table 2 lists the power reflection measurements for the different antenna scan configurations.

C. Radiometry Experiments

1) Steady State Temperature Monitoring—Fig 7(a)–(d) shows the radiometer power measured for 30 mL (V_1) urine phantom as the temperature of the urine circulating through the inflated 20 Fr Foley catheter located 35 mm from antenna surface (d_1 = 18 mm, d_2 = 35 mm) was increased from 36.5 to as high as 45°C. Fig 7(e)–(h) shows the corresponding fiberoptic temperature measurements recorded inside the urine and tissue phantoms. The form of radiometer response in Fig 7(a)–(d) is in excellent agreement with the corresponding invasive fiberoptic temperature measurements of the phantoms in Fig 7(e)–(h). Relatively constant temperatures recorded on antenna surface and fat-muscle interface in Fig 7(e)–(h) indicate very good thermal control of the circulating liquid muscle phantom surrounding the urine phantom. Fig 7 demonstrates stable system response and the ability to detect localized temperature change at depth inside well perfused kidney/muscle typically at 36.5°C using radiometry.

2) Monitoring Warm Reflux—Fig 8 shows the results of simulated kidney reflux experiments to assess the ability to detect transient reflux as the warm urine enters the highly perfused kidneys receiving 20–25% of the cardiac output at 36.5–37°C. The radiometer output shown in Fig 8 correlates very well with the seven reflux events listed in Table 1 which lasted about 50–70 seconds each. There are several interesting observations in Fig 8 and Table 1. Firstly, it should be noted that the receiver did not detect the 30 mL urine injection at the same temperature as the surrounding muscle phantom (R0). This indicates that the change in radiometer brightness temperature is predominantly associated with temperature change inside the antenna sensing volume than the change in dielectric property of the lossy tissue load at depth. Comparison of the radiometer response for 30 mL urine reflux events R1 (To=43°C) and R2 (To=45°C) suggests that the power received is directly proportional to temperature change inside the antenna sensing volume (V) for a given target volume at fixed depth. Similar observation was made for the 20 mL urine reflux events R3–R5, located at the same depth as the 30 mL refluxes. Unlike the 30 mL reflux events, relatively lower power was received for 20 mL reflux events due to the smaller target volume (R3-R5). As the urine volume was reduced to 15 and 10 mL, detectability of the reflux required higher urine temperatures (R6, R7). The highest power was recorded for the 30 mL urine reflux at 45°C (R2) and the lowest response was measured for the 10 mL reflux at 46°C (R7). Fig 8 clearly demonstrates the ability to detect transient temperature change at depth inside the kidneys using MW radiometry. However, the visibility of low reflux volumes at depth (R6, R7) requires higher temperature gradients.

IV. DISCUSSION

External bladder warming of urine to moderate hyperthermic temperatures (40–45°C) using MW hyperthermia and passive radiometric temperature monitoring of the kidneys to detect warm reflux was recently proposed for safe and noninvasive VUR detection [6,7]. The proposed radiometry diagnostic system is noninvasive and uses non-ionizing microwave radiation for gentle warming of the urine. In [7], we presented the modeling efforts for radiometer frequency selection and design of the microstrip log spiral antenna with matching layer and shield cup to acquire thermal noise radiation from the warm urine at depth. Here we evaluated the performance of the 1.375 GHz radiometer and EM shielded microstrip log spiral antenna to detect warm reflux in temperature controlled tissue mimicking phantoms.

Low viscous liquid phantoms made of ethylene glycol proposed for the bulk EM property of head and body tissues [24] and Diacetin are well suited to measure antenna receive patterns and maintain homogeneous temperature load for radiometry experiments. Phantom

NIH-PA Author Manuscript

NIH-PA Author Manuscript

formulations presented here differ in their composition and closely match the individual EM property of muscle and kidney tissues. Dielectric measurements of tissue equivalent phantoms in Fig 2 indicated good correspondence with literature data [20,27] and the human urine sample. The non-toxic liquid and solid fat phantoms were stable with long shelf life, if appropriate storing using plastic wrap (Saran®, SC Johnson, Racine, WI USA) was used. Deterioration in the dielectric property of liquid phantoms due to dehydration was easily compensated with rehydration.

Antenna return loss from the tissue load in Fig 3 indicated better than −10 dB for the 1 mm dielectric disks. However, $|S_{11}|^2$ less than −10 dB with relatively flat response was observed over the radiometer frequency band for the 0.25 mm Mylar film alone. It can be concluded that the Mylar window with permittivity close to the antenna substrate (ε'=3.66) improved antenna input matching and power reception. The use of a low loss dielectric matching layer to enhance the signal to noise ratio of the radiometric signal was also studied in [22]. The signal to ambient EMI ratio was further enhanced using a metal cup surrounding the antenna to minimize EMI (T_{EMI}) picked up by the antenna from the environment. Radiometer power spectral measurements of Fig 4 clearly demonstrated the potential EMI inside the radiometer frequency band and the shielding provided by the metal cup in continuous contact with the phantom surface and antenna ground plane. This result is of fundamental importance to translate in the clinic this EMI ultrasensitive technology.

It should be noted that the normalized volume average power density is the antenna radiometric weighting function (W) in Equation 2. of the normalized antenna power spectral density distributions of Fig 5 showed directional receive pattern with about 5% of the power density from the deep target location (30–40 mm from tissue surface). Fig 6 indicated comparable depth profiles in the power density distributions of the spiral antenna measured in the presence and absence of the metal cup. Radiometer spectral data of Fig 4 and power density distributions of Fig 6 together demonstrated that the metal cup surrounding the antenna provided effective EM shielding without deteriorating antenna power reception. EM return loss from the tissue phantom inside the scan tank was better than −10 dB for all scan configurations (Table 2).

The severity of VUR is graded I–V by the International Reflux Grading system based on the radiographic images. Grades III and above exhibit significant dilation of the ureter, renal pelvis and calyces and the degree of dilation increases for higher grade VUR. Radiometer measurements of Fig 7 clearly indicated the ability to detect temperature change of a large reflux volume (30 mL) inside the kidney, which corresponds to higher reflux grades that lasts for few minutes. Stable temperatures recorded in Fig 7 on the antenna surface and inside phantoms confirm that the radiometer response was due to localized temperature change at depth and not due to heat diffusion inside the layered phantom. Stable radiometer measurements also indicate good thermal stability of the total power radiometer. System response in Fig 7 indicates linear relation between the radiometer signal change (ΔP) and temperature differential (ΔT) of the 30 mL urine at depth.

The warm urine refluxing from the bladder comes in contact with the highly perfused kidney which receives arterial blood supply at 36.5–37°C. This could potentially accelerate heat loss into the kidney parenchyma which might degrade the ability to detect transient temperature change with MW radiometry. Thus, experiments were conducted to assess the transient response of the radiometry system to sudden temperature changes at depth. The system response of Fig 8 measured for warm urine injections followed by complete drainage clearly demonstrated the ability to detect VUR using radiometry however. The lack of change in radiometer power for the reflux event R0 in Fig 8 indicated that the signal detected during warm reflux is associated with change in temperature and not volume. Fig 8 also indicated smaller signal changes for lower reflux volumes (R2 vs. R7) and lower urine temperatures (R1 vs. R2). This is because the brightness temperature ($T_{B,\,i}$) given in Eqn (2) is related to phantom temperature and the ratio of power received from the refluxed urine volume at depth to the power received from the total sensing volume as discussed in [38]. Furthermore, the power gathered by the antenna reduces with increase in target depth (d_1) and, decrease in target volume (V_1) and urine temperature (T_0). Radiometer response of Fig 8 clearly demonstrated that warm reflux on the order of 20–30 mL can be detected using MW radiometry (R1–R5) and the visibility of smaller and deeper refluxes could be challenging (R6, R7). Efforts to improve system sensitivity to detect lower grade reflux are underway. System design is also being improved to address the influence of internal organ motion, reliable antenna positioning for kidney temperature monitoring and, miniaturization of the antenna and receiver for clinical implementation. Following successful system characterization in tissue phantoms, efforts are being focused on conducting animal experiments to evaluate the clinical potential of the proposed technique for non-invasive detection of VUR.

V. CONCLUSION

MW radiometry for passive temperature monitoring of the kidney region to detect the reflux of warm urine from the bladder to kidneys during external bladder warming is evaluated in temperature controlled phantoms with tissue equivalent EM properties. Thin dielectric matching layers are investigated to enhance power reception from the target and a metal cup is used to improve receiver signal to ambient EMI ratio. An EM shielded log spiral antenna is shown to provide a directional receive pattern in the radiometer frequency band. Radiometer system response in tissue phantoms indicate the ability to reliably detect warm VUR at depth using the 1.375 GHz total power radiometer connected to an EM shielded microstrip log spiral antenna. Experimental characterization of the radiometry system in tissue phantoms evaluated for the conditions of this study clearly demonstrates the promise of this non-invasive safe and cost-effective diagnostic test for VUR detection.

Acknowledgments

The authors would like to acknowledge support of this research by ThermImage Corporation and generous support from Agilent Technologies (Michael Hoffman and Stan Mills), Aprel Laboratories (Stuart Nicol), Emmerson & Cummings (James DelPrete) and National Instruments (Troy Matus). Special thanks to Don Pearce at Duke University Medical Workshop Center. We also acknowledge NIH grants R44CA104061, RO1-CA70761 and P01-CA-042745-22.

REFERENCES

1. Sargent MA. What is the normal prevelance of vesicoureteral reflux? Pediatric Radiology. 2000; 30:587–593. [PubMed: 11009294]
2. Pediatrics AA. Practice parameter: the diagnosis, treatment, and evaluation of the initial urinary tract infection in febrile infants and young children. Pediatrics, Committee on Quality Improvement, Subcommittee on Urinary Tract Infection. 1999; 103:843–852.
3. Darge K, Riedmiller H. Current status of vesicoureteral reflux diagnosis. World J Urology. 2004; 22:88–95.
4. Traxel E, et al. Risk factors for urinary tract infections after dextranomer/hyaluronic acid endoscopic injection. Journal of Urology. 2009; 182:1708–1713. [PubMed: 19692024]
5. Brenner DJ, et al. Estimated risks of radiation-induced fatal cancer from pediatric CT. American J Roentgenology. 2001; 176:289–296.
6. Snow W, Taylor M. Non-Invasive Vesicoureteral Reflux Imaging. J Pediatric Urology. 2010 accepted in.

7. Arunachalam K, et al. Modeling the detectability of vesicoureteral reflux using microwave radiometry. Phys. Med. Biol. 2010; 55(18)
8. Cheever EA, Foster KR. Microwave radiometry in living tissue: what does it measure? IEEE Transactions on Biomedical Engineering. 1992; 39(6):563–568. [PubMed: 1601437]
9. Leroy Y, Bocquet B, Momouni A. Non-invasive microwave radiometry thermometry. Physiol. Measurements. 1998; 19:127–148.
10. Ulaby, FT.; Moore, RK.; Fung, AK. Microwave Remote Sensing, Active and Passive. Microwave Remote Sensing Fundamentals and Radiometry, Volume I. Artech House; 1981.
11. Land DV. An efficient, accurate and robust radiometer configuration for microwave temperature measurement for industrial and medical applications. Journal of microwave power and electromagnetic energy. 2001; 36(3):139–153. [PubMed: 11837048]
12. Bardati F, Iudicello S. Modeling the Visibility of Breast Malignancy by a Microwave Radiometer. IEEE Transactions on Biomecial Engineering. 2008; 55(1):214–221.
13. Lee JW, et al. Experimental investigation of the mammary gland tumour phantom for multifrequency microwave radio-thermometers. Medical & biological engineering & computing. 2004; 42(5):581–590. [PubMed: 15503957]
14. Mouty S, et al. Microwave radiometric imaging (MWI) for the characterisation of breast tumours? The European Physical Journal Applied Physics. 2000; 10:73–78.
15. Hand JW, et al. Monitoring of deep brain temperature in infants using multi-frequency microwave radiometry and thermal modelling. Physics in Medicine and Biology. 2001; 46:1885–1903. [PubMed: 11474932]
16. Ohba H, et al. Multifrequency microwave radiometry for non-invasive thermometry using a new temperature profile model function. IEICE Transactions on Electronics. 1995; E78-C(8):1071–1081.
17. Arunachalam K, et al. Characterization of a digital microwave radiometry system for noninvasive thermometry using a temperature-controlled homogeneous test load. Physics in Medicine and Biology. 2008; 53(14):3883–3901. [PubMed: 18591733]
18. Jacobsen S, Stauffer PR. Can we settle with single-band radiometric temperature monitoring during hyperthermia treatment of chestwall recurrence of breast cancer using a dual-mode transceiving applicator? Physics in Medicine and Biology. 2007; 52:911–928. [PubMed: 17264361]
19. Jacobsen S, Stauffer PR, Neuman DG. Dual-mode antenna design for microwave heating and noninvasive thermometry of superficial tissue disease. IEEE Transactions on Biomedical Engineering. 2000; 47(11):1500–1509. [PubMed: 11077744]
20. Dietsch A, et al. Microwave Thermochemotherapy in the Treatment of the Bladder Carcinoma—Electromagnetic and Dielectric Studies—Clinical Protocol. IEEE Transactions on Biomedical Engineering. 2000; 47(5):633–641. [PubMed: 10851807]
21. Despretz D, et al. Microwave Prostatic Hyperthermia: Combination-Theoretical Study Interest of Urethral and rectal Applicators combination - Theoretical and Animal Experimental Results. IEEE Transactions on Microwave Theory and Techniques. 1996; 44(10):1762–1768.
22. Karanasiou IS, et al. Development and Laboratory Testing of a Noninvasive Intracranial Focused Hyperthermia System. IEEE Transactions on Microwave Theory and Techniques. 2008; 56(9): 2160–2171.
23. Karanasiou IS, Papageorgiou C, Uzunoglu NK. Is it possible to measure non-invasively brain conductivity fluctuations during reactions to external stimuli with the use of microwaves? International Journal of Bioelectromagnetism. 2005; 7(1):356–359.
24. Kanda MY, et al. Formulation and Characterization of Tissue Equivalent Liquids Used for RF Densitometry and Dosimetry Measurements. IEEE Trans. Microwave Theory Techniques. 2004; 52(8):2046–2056.
25. Poppendiek HF, et al. Thermal conductivity measurements and predictions for biological fluids and tissues. Cryobiology. 1966; 3(4):318–327.
26. Wyatt C, et al. Hyperthermia MRI Temperature Measurement: Evaluation of Measurement Stabilization Strategies. Int J Hyperthermia. 2009; 25(6):422–433. [PubMed: 19925322]

27. Gabriel S, Lau RW, Gabriel C. The dielectric properties of biological tissues: III. Parametric models for the dielectric spectrum of tissues. Physics in Medicine and Biology. 1996; 41:2271–2293. [PubMed: 8938026]

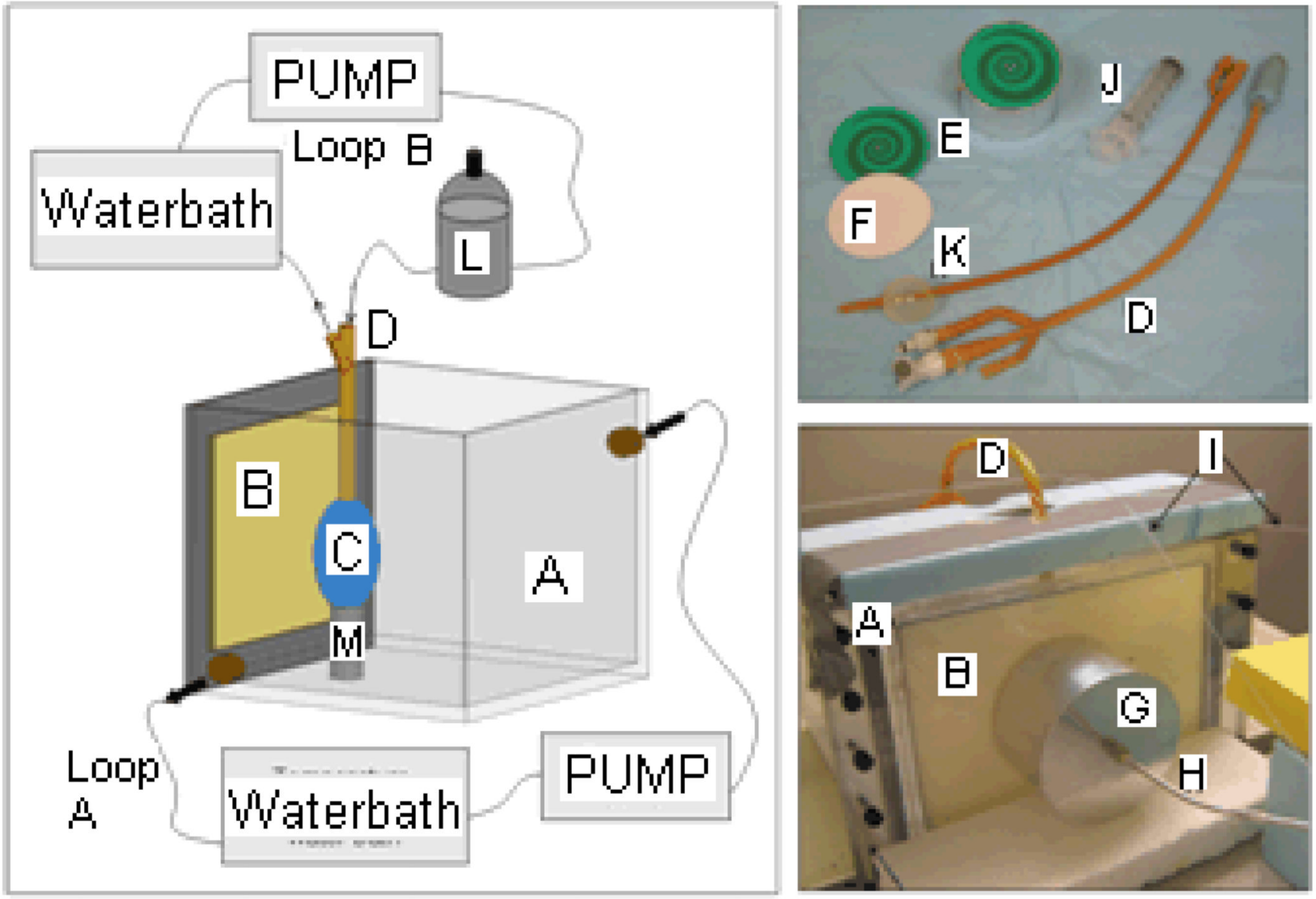

Fig. 1.

Experimental setup for radiometric temperature monitoring of kidney model. Liquid muscle phantom inside the insulated acrylic container (A) with 5 mm overlying fat phantom (B) was circulated through temperature-controlled water bath using peristaltic pump (loop A). Temperature controlled urine phantom was circulated through the Foley catheter rigidly suspended inside the muscle phantom (loop B). Thermal noise radiation from the layered phantom gathered by the radiometric antenna (E) inside metal cup (G) positioned on a Mylar window of the muscle filled chamber (A) is measured by a total power radiometer connected to the antenna via semi rigid coaxial cable (H). A: acrylic container; B: 5 mm layer of solid fat phantom ; C: inflated latex pouch around the 20 French 3-way Foley catheter (D); E: microstrip log spiral antenna; F: 80 mm dia and 1 mm thick Eccostock® dielectric matching layer; G: metal cup; H: low loss semi rigid coaxial cable; I: Fiberoptic temperature sensors; J: Syringe; K: 18 French/2-way straight tip Foley catheter with 30 mL balloon; M: perforated plastic support.

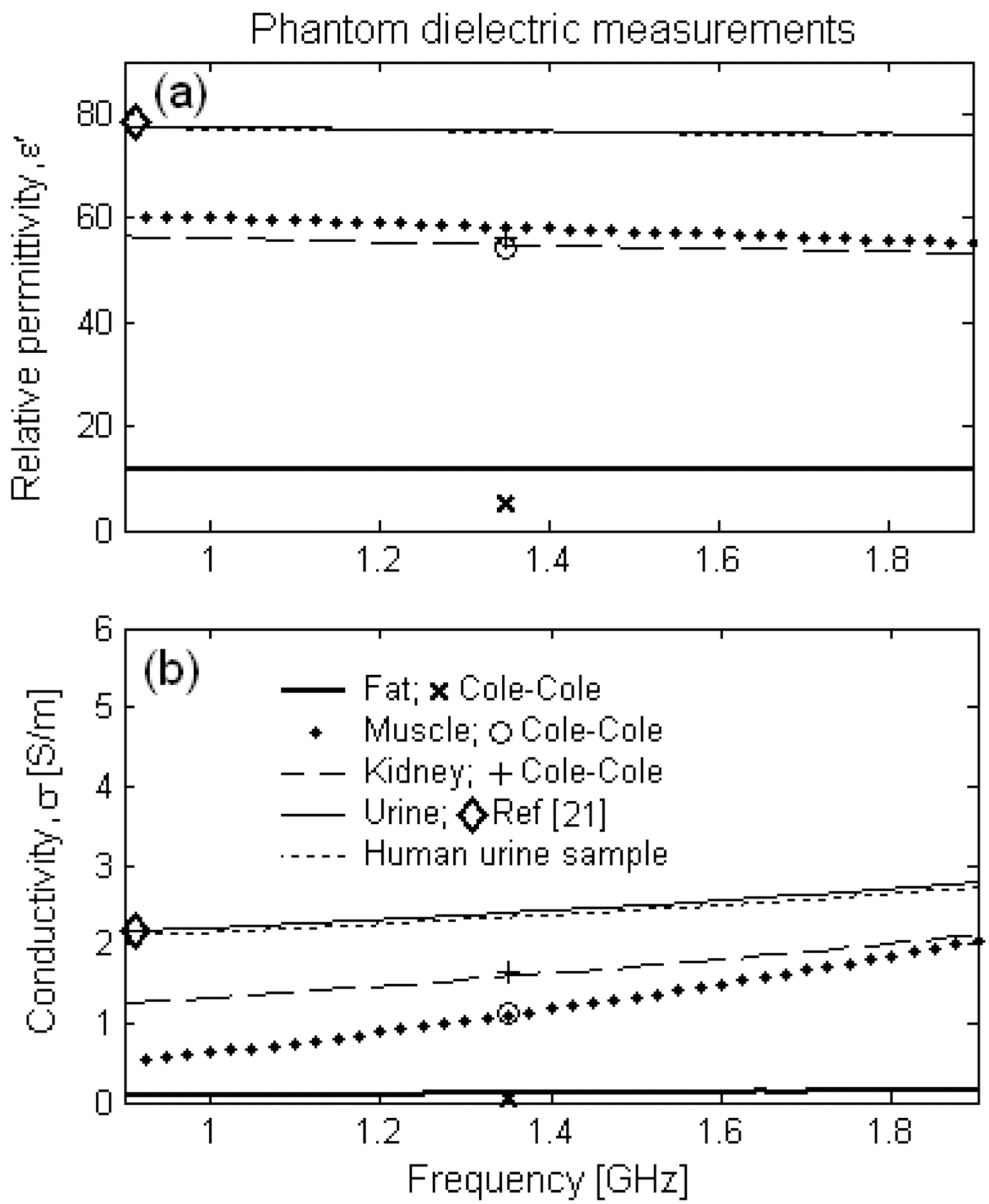

Fig. 2.
Dielectric measurements of fat, muscle (DGBE), kidney (Diacetin) and urine phantoms at room temperature (23°C). Symbols indicate Cole-Cole [27] values at the radiometer center frequency and urine data from [20].

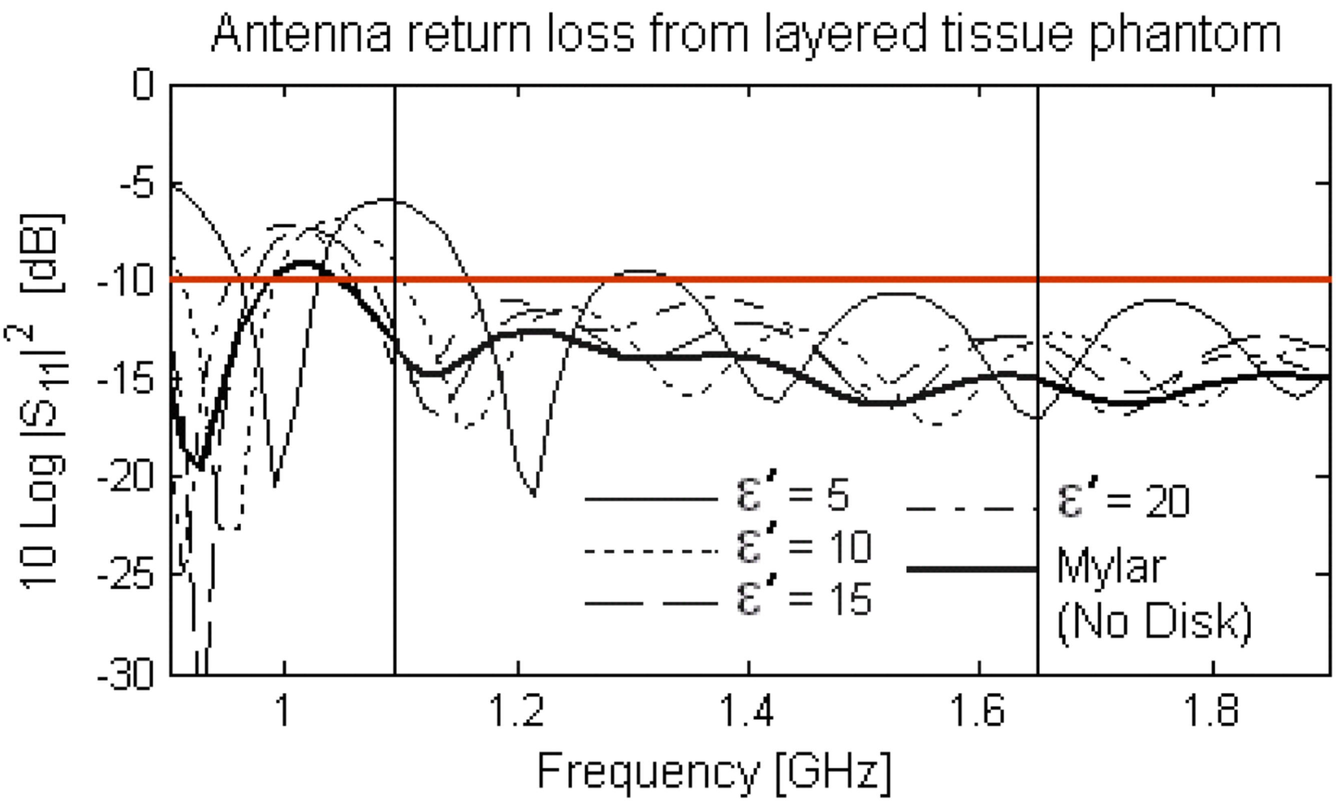

Fig. 3.
Antenna return loss for 1 mm Eccostock dielectric disk of varying permittivity between the antenna and tissue load through the Mylar window. Relatively flat response (better than −10 dB) was observed for the 0.25 mm Mylar film.

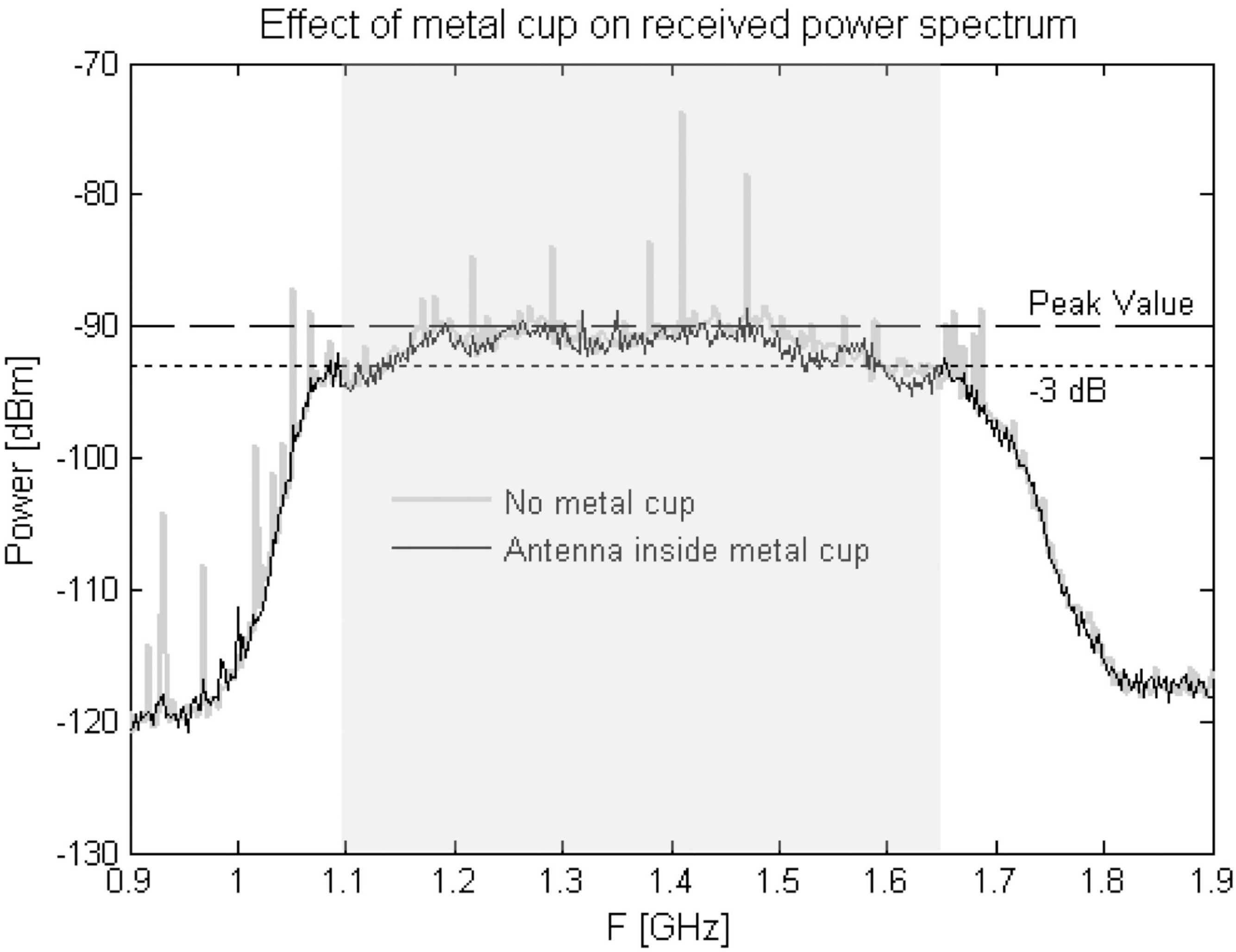

Fig. 4.
Radiometer power spectrum with the antenna in continuous contact with the layered tissue phantom. The metal cup surrounding the antenna significantly reduced EMI peaks in the radiometer frequency band (1.1–1.6 GHz).

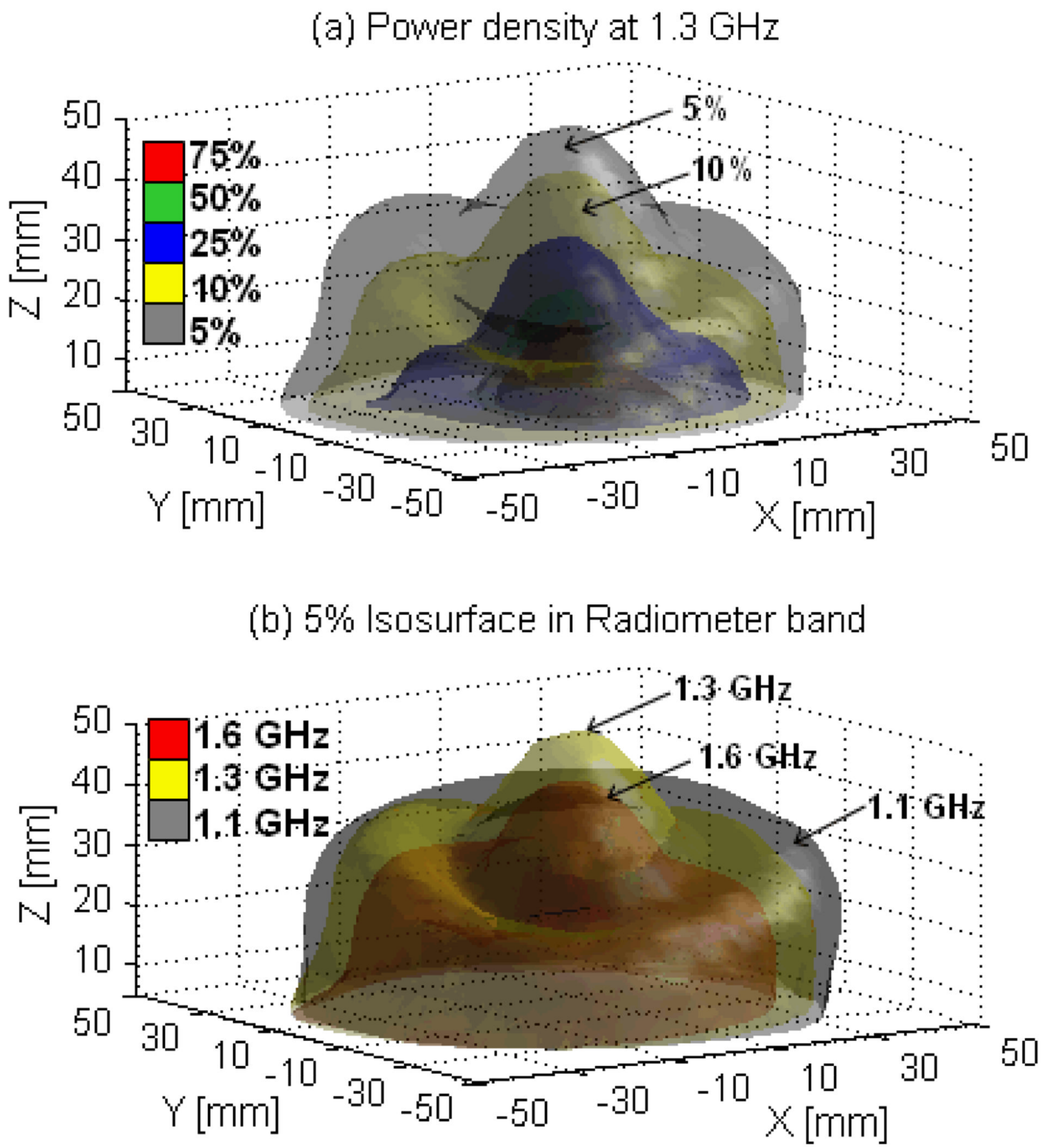

Fig. 5.

Power spectral density of log spiral measured inside the liquid muscle phantom. (a) Isosurfaces measured at 1.3 GHz (b) Comparison of the 5% isosurfaces in the radiometer frequency band (1.1–1.65 GHz). Measurements were normalized with respect to the maximum value recorded at z=5 mm plane. Note that power density at the target depth (30–50 mm) is about 5%.

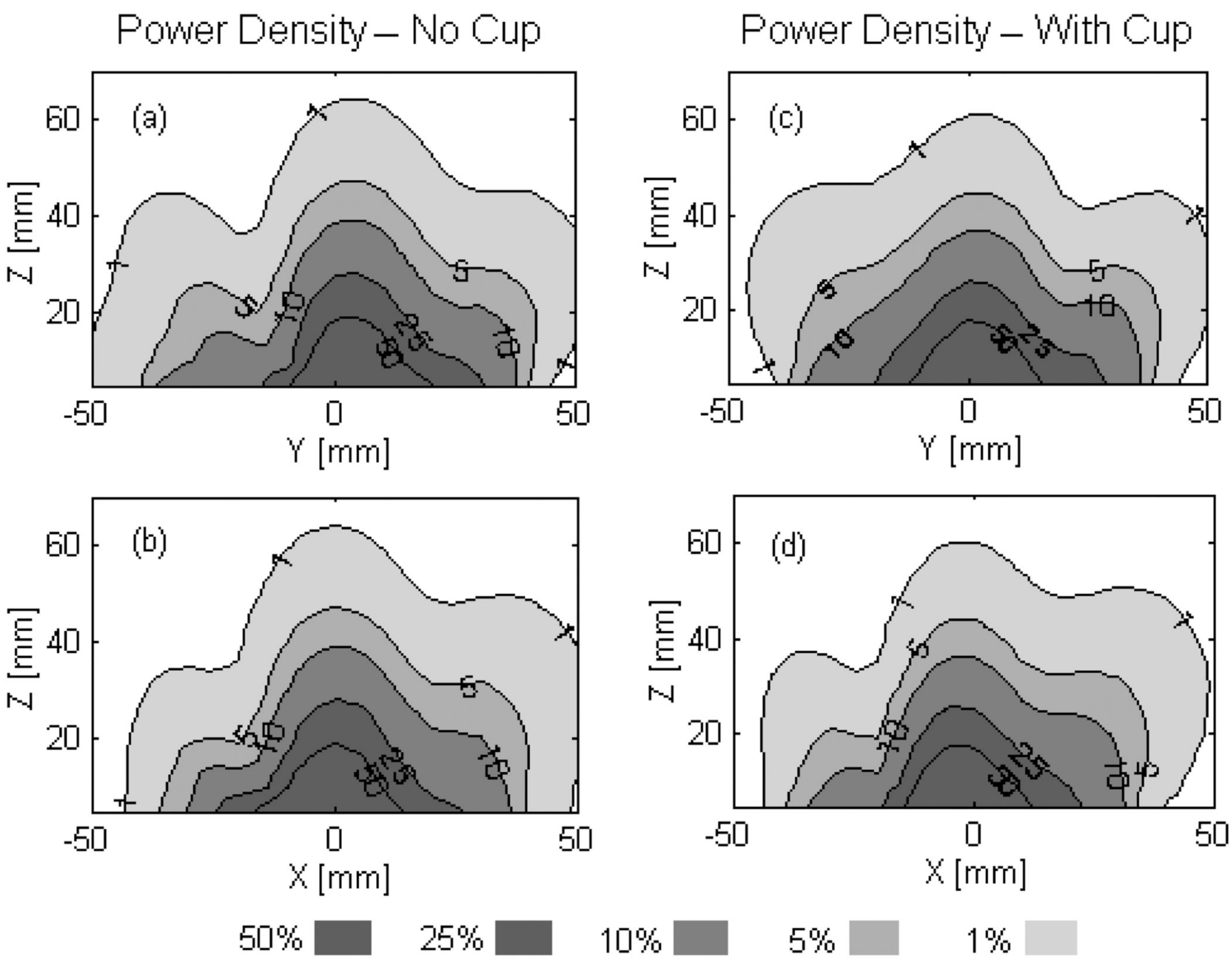

Fig. 6.
Comparison of normalized power density measured in the orthogonal planes at 1.3 GHz with (c–d) and without (a–b) metal cup surrounding the antenna. Power density is normalized with respect to the maximum value in z=5 mm plane in the scant tank with muscle phantom. The antenna receive patterns are not significantly affected in the presence of metal cup.

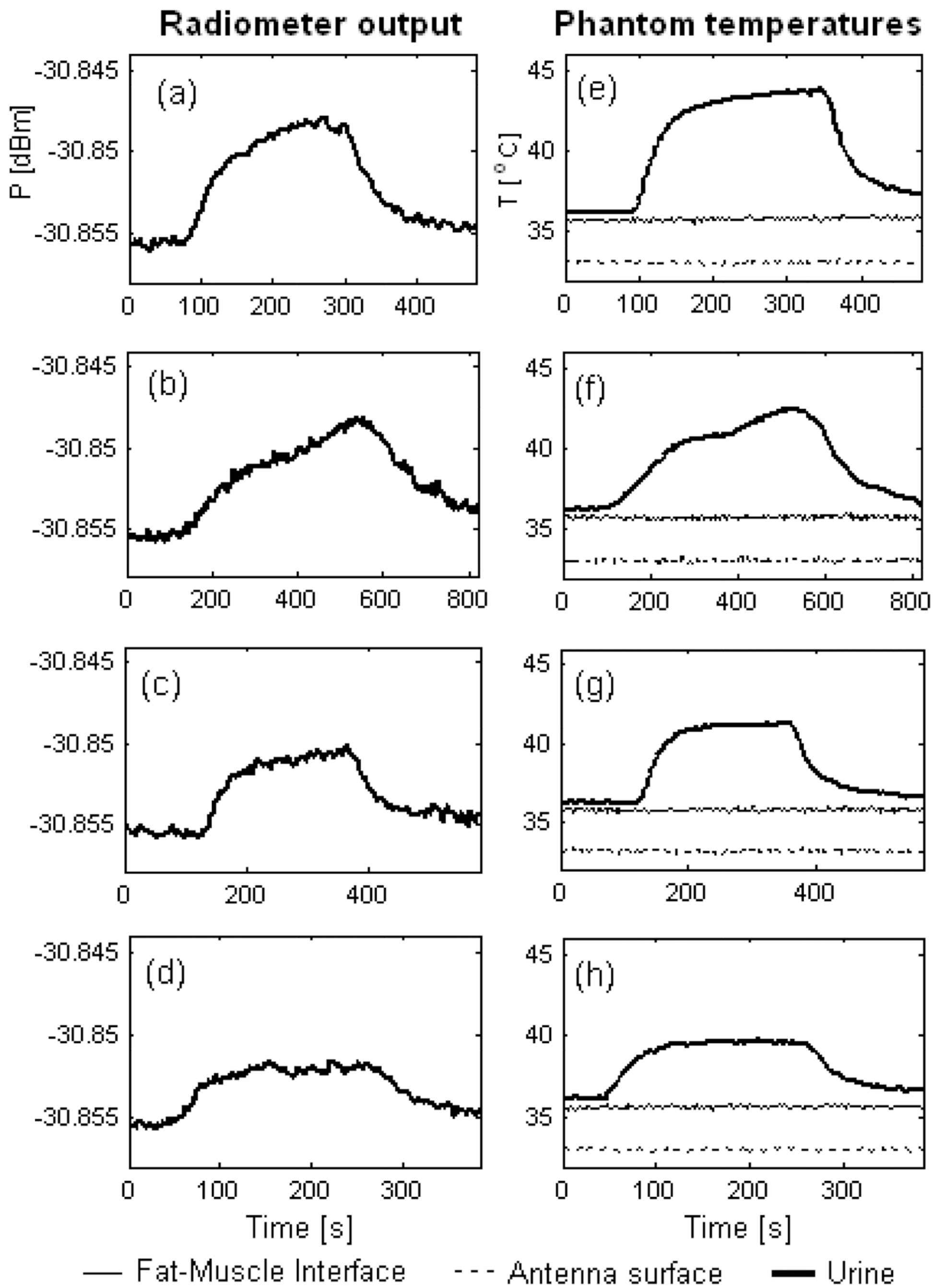

Fig. 7.

Radiometer and phantom temperature measurements acquired during steady state temperature monitoring experiments. The temperature of the 30 mL circulating urine phantom was increased 3–8°C above the surrounding muscle phantom maintained at 36.5°C. Radiometer output correlates very well with the temperature of the urine phantom, with its center located 35 mm (d_2) from the antenna surface.

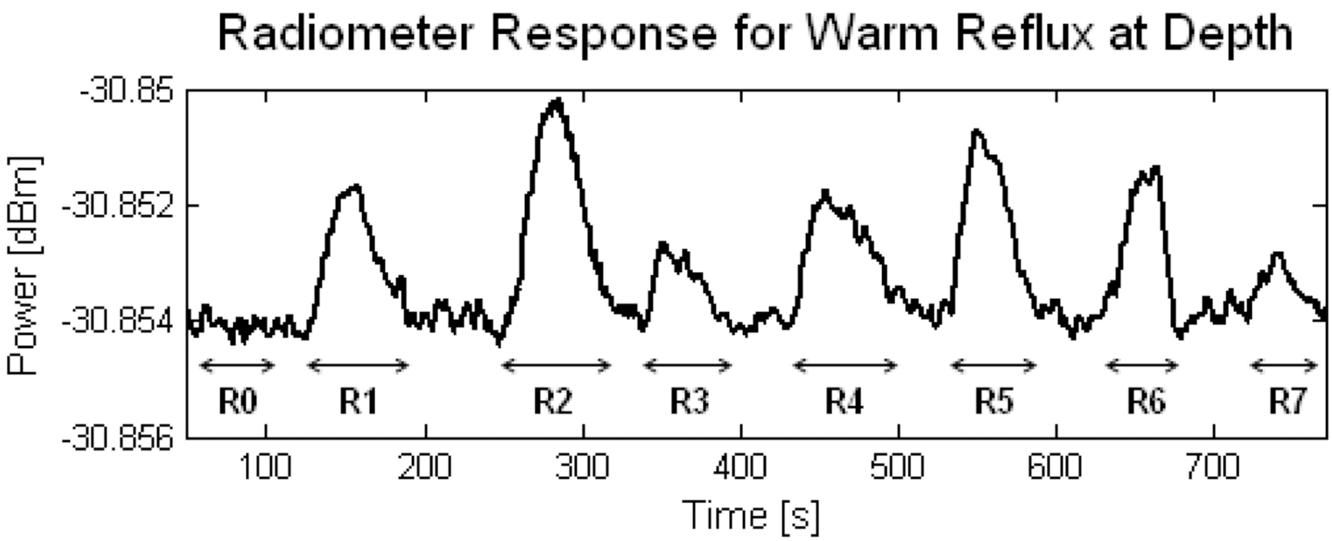

Fig. 8.
Radiometer measurements through the layered tissue load for warm urine injections of varying volume (10–30 mL) and temperature (39.5–46°C) at 35 mm depth inside the highly perfused 36.5°C lossy muscle/kidney phantom (Table 1). Note that the highest radiometer power level is recorded for the largest reflux volume at the highest urine temperature (R2).

TABLE I

Kidney reflux experiments for warm urine injections. Antenna-to-Foley center distance d_2=35 mm; antenna surface temperature = 33.9°C; muscle phantom = 36.5°C.

Reflux Event	Reflux volume (V_1) [mL]	Antenna to Foley front surface (d_1) [mm]	Urine temperature before injection (T_0) [°C]
R0	30	17	36.2
R1	"	"	43.0
R2	"	"	45.0
R3	20	20	39.5
R4	"	"	41.5
R5	"	"	44.0
R6	15	22	46.0
R7	10	23	46.0

TABLE II

Power delivered and reflected by the antenna from the scan tank filled with liquid muscle phantom for different antenna scan configurations.

Frequency [GHz]	Antenna forward power [W]	Antenna $\lvert S11\rvert^2$ [dB]	Scan setup
1.1	4.78	-10.86	no metal cup
1.3	4.70	-12.45	"
"	"	-17.25	metal cup
1.6	4.20	-12.06	no metal cup